(12) INTERNATIONAL APPLICATION PUBLISHED UNDER THE PATENT COOPERATION TREATY (PCT)

(19) World Intellectual Property Organization
International Bureau

(43) International Publication Date
15 February 2018 (15.02.2018)

W!P O I PCT

(10) International Publication Number
WO 2018/031148 Al

(51) International Patent Classification:
*G21C 1/22* (2006 .0 1) *G21C 7/26* (2006 .01)

(21) International Application Number:
PCT/US2017/040833

(22) International Filing Date:
06 July 2017 (06.07.2017)

(25) Filing Language: English

(26) Publication Langiuage: English

(30) Priority Data:
62/358,993 06 July 2016 (06.07.2016) U S

(71) Applicant: **TRANSATOMIC POWER CORPO¬RATION** [US/US]; One Broadway, 14th Floor, Cam¬bridge, Massachusetts 02142 (US).

(72) Inventors: **ROBERTSON, Sean;** 372 Marlborough Street, Apt. #6, Boston, Massachusetts 021 15 (US). **MASSIE, Mark;** 2 3 Sidney Street, Apt. 414, Cambridge, Massachu¬setts 02139 (US). **SMITH, Stephen;** 171 Lions Mouth Road, Amesbury, Massachusetts 01913 (US). **DEWAN, Leslie C ;** 2 3 Sidney Street, Apt. 414, Cambridge, Massa¬chusetts 02139 (US).

(74) Agent: **DEAN, Sean** et al; Fish & Richardson P.C., P.O. Box 1022, Minneapolis, Minnesota 55440-1022 (US).

(81) Designated States *(unless otherwise indicated, for every kind of national protection available):* AE, AG, AL, AM, AO, AT, AU, AZ, BA, BB, BG, BH, BN, BR, BW, BY, BZ, CA, CH, CL, CN, CO, CR, CU, CZ, DE, DJ, DK, DM, DO, DZ, EC, EE, EG, ES, FI, GB, GD, GE, GH, GM, GT, HN, HR, HU, ID, IL, IN, IR, IS, JO, JP, KE, KG, KH, KN, KP, KR, KW, KZ, LA, LC, LK, LR, LS, LU, LY, MA, MD, ME, MG, MK, MN, MW, MX, MY, MZ, NA, NG, NI, NO, NZ, OM, PA, PE, PG, PH, PL, PT, QA, RO, RS, RU, RW, SA, SC, SD, SE, SG, SK, SL, SM, ST, SV, SY, TH, TJ, TM, TN, TR, TT, TZ, UA, UG, US, UZ, VC, VN, ZA, ZM, ZW.

(84) Designated States *(unless otherwise indicated, for every kind of regional protection available):* ARIPO (BW, GH, GM, KE, LR, LS, MW, MZ, NA, RW, SD, SL, ST, SZ, TZ, UG, ZM, ZW), Eurasian (AM, AZ, BY, KG, KZ, RU, TJ, TM), European (AL, AT, BE, BG, CH, CY, CZ, DE, DK, EE, ES, FI, FR, GB, GR, HR, HU, IE, IS, IT, LT, LU, LV, MC, MK, MT, NL, NO, PL, PT, RO, RS, SE, SI, SK, SM, TR), OAPI (BF, BJ, CF, CG, CI, CM, GA, GN, GQ, GW, KM, ML, MR, NE, SN, TD, TG).

**Published:**
— *with international search report (Art. 21(3))*
— *before the expiration of the time limit for amending the claims and to be republished in the event of receipt of amendments (Rule 48.2(h))*

(54) Title: CONTROLLING REACTIVITY IN MOLTEN SALT REACTORS

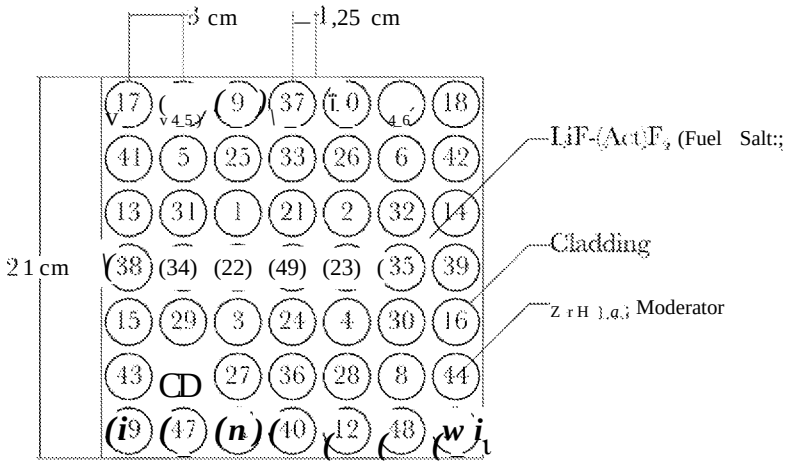


Figure 11

(57) Abstract: A molten salt reactor design employs continuous fission product removal and core geometry modification to achieve high fuel utilization

W o 2018/031148 A1

# Controlling Reactivity in Molten Salt Reactors

## TECHNICAL FIELD

This invention relates to nuclear reactors, and more particularly to molten salt reactors.

## BACKGROUND

Nuclear energy is an ideal alternative to fossil fuels and is a well-characterized technology that can generate a large baseload supply of carbon-free electricity at minimal operating cost. However, the nuclear power industry has historically been hampered in part by concerns about legacy technology's production of nuclear waste. To address this concern, multiple advanced reactor technologies feature innovative designs that are capable of consuming nuclear waste, recovering much of the energy that legacy reactors leave behind. One of these technologies, the molten salt reactor (MSR), was first developed at the Oak Ridge National Laboratory in the 1950s and 1960s, and is a reactor design that utilizes liquid fuel.

## SUMMARY

The nuclear reactor designs described in this document address existing concerns about waste storage by increasing fuel utilization and reducing overall waste production. The molten salt reactor design described in this document takes advantage of its liquid fuel in order to address these challenges. By employing continuous fission product removal and core geometry modification, the described MSR achieves more than twice the fuel utilization of light water reactors (LWRs). When using 5% enriched uranium – the maximum enrichment readily available in the current supply chain – this increased efficiency leads to an approximate 55% waste reduction compared to LWRs. Using higher enrichments, up to the 20% Low Enriched Uranium (LEU) limit, this reduction reaches 83%.

This design uses a particular moderator and fuel salt to attain criticality using both low-enriched uranium fuel and the remaining fissile material in light water reactor (LWR) spent nuclear fuel (SNF). This document describes the reactor physics and operational characteristics of the designs. This reactor can reduce reactor waste production by increasing fuel burnup. Burnup, also known as fuel utilization, is

defined as the thermal energy extracted per unit mass of heavy metal, typically given in units of GWd/MTHM, where MTHM stands for Metric Tons of Heavy Metal.

The typical definition of fuel burnup is given by the following equation:

$$Bu = \frac{P \cdot t}{m_i}$$

in which $Bu$ is the burnup, $P$ is the reactor's thermal power, $t$ is the fuel residence time, and $m_i$ is the initial actinide loading in the reactor. In liquid fueled reactors, it is necessary to modify this equation to take into account the additional mass of actinides $m_a$ added to the reactor over the course of operation:

$$Bu = \frac{P \cdot t}{m_i + m_a}$$

The design incorporates a new method of moderator rod operation that minimizes excess reactivity in the core, allowing for considerably higher burnup than light water reactors and decreased waste production. Reactivity, $\rho$, is defined by the equation,

$$\rho = \frac{k_{eff} - 1}{k_{eff}}$$

in which keff is the reactor's effective multiplication factor, the ratio of neutron populations from one neutron life cycle to the next.

The details of one or more embodiments of the invention are set forth in the accompanying drawings and the description below. Other features, objects, and advantages of the invention will be apparent from the description and drawings, and from the claims.

## DESCRIPTION OF DRAWINGS

Figure 1 shows the infinite multiplication factor, $k\infty$, as a function of burnup, illustrating the effects of fission product removal on two otherwise identical systems. The dashed line for a $k\infty$ of 1.018 indicates the point at which the reactor can no longer sustain the fission chain reaction when taking into account radial and axial leakage.

Figure 2 shows a graphical depiction of reactivity swing, adapted from Cochran and Tsoulfanidis, 1990. As fissile material is consumed throughout the course of operation, the extent to which positive reactivity exists in the core

diminishes, up until the point at which criticality ($\rho = 0$) is no longer achievable (maximum burnup).

Figure 3 shows the infinite multiplication factor as a function of `SVF' and 235U enrichment. The expected operational progression of `both a stationary rod configuration (I., vertical) and moveable rod configuration (II., horizontal)' have been presented through the use of `dashed lines. Additional simulation details are given in Appendix A.

Figure 4 shows conversion ratio as a function of `SVF' and `235U enrichment. SVF was modified by changing the moderator rod radius. The expected operational progression of `both a stationary rod configuration (I., vertical)' and `moveable rod configuration (II, horizontal) have been presented through the use of `dashed lines.

Figure 5 shows a conceptual depiction of `a reactor core design that uses moveable moderator rods for reactivity control. The gap between the moderated region and the reactor vessel wall contains unmoderated fuel salt that acts as both a reflector and fertile nuclei conversion zone.

Figure 6 shows the change in `SVF' as a function of `burnup' in the reactor for a 5% enriched initial fuel load. The legend refers to the two analyzed `feed compositions: 5% enriched and SNF. Additional calculation details are given in Appendix A.

Figure 7 shows fissile atom density as a function of `burnup' for the representative reactor operation. The legend refers to the two analyzed `feed compositions: 5% enriched and SNF. The data represent a summation of `the 235U, 239Pu, and 241Pu atom densities, with their respective individual trends being given in Appendix C.

Figure 8 shows conversion ratio as a function of `burnup' for the representative reactor operation. The legend refers to the two analyzed `feed compositions: 5%, enriched and SNF. Additional calculation details are given in Appendix A.

Figure 9 shows annual actinide waste production as a function of `burnup', normalized to a 1250 MWth power level. The legend indicates `feed compositions' of `Low Enriched Uranium (LEU) and SNF.

Figure 10. Burnup (left, light) and normalized waste production (right, dark) for the examined fuel cycles, normalized to a 1250 MWth power level.

Figure 11 shows radial cross section of the assembly simulated in Serpent 2.26. The numbers located in the center of each rod indicate the insertion order used throughout the report, with 1 indicting the 1st rod inserted and 49 the last.

Figure 12 shows normalized neutron flux per lethargy as a function of energy at the beginning of life (BOL) and end of life (EOL). The spectra were taken from the depletion results of the 5% LEU initial load / 5% feed fuel cycle trial.

Figure 13 shows assembly level k∞ limit as a function of the number of rods inserted. Assemblies are comprised of a 7-by-7 array of ZrH1.66 moderator rods.

Figure 14 shows a radial cross section of the EOL full core model used in the leakage calculations.

Figure 15 shows full core radial flux profile for a 5% enriched initial actinide load.

Figure 16 shows Shannon entropy as a function of the number of inactive cycles for the full core leakage calculations.

Figure 17 shows the evolution of several primary fissile and fertile isotopes for the 5% initial load / 5% feed depletion simulation.

Like reference symbols in the various drawings indicate like elements.

## DETAILED DESCRIPTION

### *Fuel Utilization in Liquid-Fueled Reactors*

Nuclear fuel burnup is a key parameter for measuring the efficiency of the nuclear fuel cycle. A higher-burnup fuel cycle decreases waste production, and thus potentially reduces long-term waste storage costs and environmental impact. Increasing burnup is equivalent to increasing the amount of time that a reactor maintains criticality with a given amount of fuel, which is typically accomplished by having either a large initial loading of fissile material, or a high conversion of fertile to fissile nuclei in the reactor. The main factors limiting fuel burnup in light water reactors are structural damage and trapping of fission products in the solid fuel pellets. Over the course of operation, fission product buildup within the rods can reduce the fuel pellets' thermal conductivity, thereby increasing the rod's centerline temperature and decreasing the margin to the fuel's melting point. Increased fuel temperature and radiation-induced damage can lead to swelling in the fuel pellets, which in turn can cause the fuel pellets to impinge on the cladding and, in extreme cases, lead to

cladding failure. Buildup of fission products within the fuel rods also reduces the system's reactivity over time, because of several isotopes' high neutron absorption cross sections.

### *Fission Product Removal and Reactor Fuel Utilization*

In contrast to solid fuel, liquid fuel has numerous advantages that allow for increased fuel burnup. Liquid fuel has no long-range structure to be damaged, does not experience significant volumetric swelling, and avoids fission product poisoning through continuous fission product removal. To measure quantitatively the effect of fission product removal in molten salt systems, two depletion calculations[1] on otherwise identical models were run using the neutronics software Serpent 2.26. The results of the simulation can be seen in Figure 1, with additional parameters given in Appendix A.

Although fission product removal increases the maximum burnup by more than 27% (44.5 GWd/MTHM compared to 34.8 GWd/MTHM), the final value still falls short of yielding significant improvements when compared to current LWR limits (45 GWd/MTHM). To increase this value further, it is possible to take advantage of another aspect of liquid fueled reactors: the ability to easily vary their geometry, by inserting or removing moderator rods in the reactor core.

### *A New Take on Reactivity Control*

In order to account for the loss of fissile material over the course of operation, solid-fueled nuclear reactors use core configurations and fuel compositions that result in excess positive reactivity at the beginning of life. During normal operation, excess reactivity is accounted for using control rods and soluble absorbers – the additional neutrons are captured, and the reactor can be operated safely.

The concept of "reactivity swing" (the variation in reactivity in a reactor over the course of a given fuel loading) is shown graphically in Figure 2. A reactor with a large reactivity swing is inherently inefficient, as neutrons that could have otherwise been used for fission and conversion in the fuel are effectively wasted in the absorbers and control rods. An ideal reactor therefore has minimal reactivity swing, and can use its neutron population with the greatest efficiency during operation.

[1] Depletion calculations are computer simulations that model burnup over the course of the reactor's life.

The neutron balance in a reactor is a function of both geometry and core material composition. In solid-fueled reactors, geometry is largely fixed, and control is achieved through modifications in the composition – insertion and removal of neutron absorbing material. Liquid-fueled reactors, however, make it possible to control reactivity by altering the core's geometry, thereby largely eliminating reactivity swing in the system. Specifically, it is possible to readily vary the salt volume fraction (SVF; the percentage of the core volume occupied by fuel salt) in an MSR core by inserting or removing moderator rods. In order to illustrate the effect of changing SVF in the core, a scoping study consisting of multiple steady state pin cell calculations was performed in Serpent 2.26.

Varying the levels of $^{235}$U enrichment (1 – 5%) and modifying SVF through the simulation of different-sized moderator rods makes it possible to estimate the evolution of the fuel with time. Figure 3 shows a plot of infinite multiplication factor as a function of SVF for these multiple enrichment levels. The graph shows that as fissile material concentration in the reactor decreases, the reactor can either maintain criticality:

I. By beginning with a large amount of excess reactivity and a constant SVF, as in a stationary moderator rod configuration, or,

II. By decreasing SVF, as in a moveable moderator rod configuration.

Although exact operational progression cannot be derived from this graph, since the simulations do not take into account the generation of transuranic isotopes over the course of life, the general relationships among fissile concentration, multiplication factor, and SVF can be inferred.

From this trend, it can be seen that it is possible to control the system's reactivity by adjusting the reactor's SVF. Such an adjustment can thus be used to eliminate reactivity swing, thereby increasing the reactor's neutron utilization efficiency and conversion ratio. Figure 4 illustrates this effect through a plot of conversion ratio as function of enrichment and SVF. The graph demonstrates that as fissile material concentration decreases, moving from higher to lower SVF does, in fact, produce a higher conversion ratio over the course of life (II) than does a stationary rod configuration (I).

In practice, SVF will be varied by inserting fixed-sized moderator rods via the bottom of the reactor vessel (for safety considerations), in a manner analogous to moving the control rods in a boiling water reactor, as shown in Figure 5. The reactor

therefore does not require control rods beyond a single shutdown rod for safety. As an additional shutdown mechanism, moderator rod removal may also act as a means of bringing the reactor into a subcritical state.

### *Depletion Calculations with Movable Moderator Rods*

The scoping calculations make it possible to infer the influence of SVF on burnup and reactivity control in an MSR. Following this initial scoping, assembly level depletion calculations were used to simulate the system evolution over time to a higher degree of accuracy. In these simulations, SVF was adjusted to minimize excess reactivity. The model employs continual fission product removal and a fuel addition method that maintains absolute actinide concentration following each time step.[2] The initial actinide loading is comprised of 5% LEU, with two different feed compositions being used for comparison: one consisting of 5% LEU, and the other consisting of 50 GWd/MTHM SNF.

Figure 6 shows the change in SVF in the reactor as a function of burnup for both feed compositions. At the beginning of life, a high SVF is used to harden the spectrum [3] and convert the maximum amount of fertile material while the fissile content is still high. As shown in Figure 7, as fissile concentration begins to drop additional moderator rods are inserted in order to maintain criticality, leading to a decrease in SVF and subsequently conversion ratio (Figure 8).

As the final mass of feed in these simulations is small in comparison to the initial actinide load, the small difference between the two fuel cycles is caused by the slight difference in feed composition. Specifically, the fissile concentration of the feed material has a direct influence on conversion ratio, as it can be thought of as an additional fissile production term. Equation 1 illustrates this effect by presenting an effective conversion ratio ($CR_{eff}$), defined as the system's conversion ratio (CR) plus the fissile concentration of the feed (FFeed).

$$CR_{eff} = CR + F_{Feed} \quad (1)$$

[2] In an operating MSR, it is necessary to add additional actinide fuel to the system so that the fuel salt can remain at its eutectic composition. Additionally, further details on fission product removal are included in Appendix A.

[3] Also note that at the beginning of life, leakage in the system is approximately 4.3 %, dropping to 1.8% by the end of life. Leakage considerations are described in more detail in Appendix B.

### *Waste Reduction and Consuming SNF*

Addressing nuclear energy's major challenge of long-lived waste disposal requires two substantial steps, as the industry must both reduce the rate at which waste is produced and find a long-term solution for the world's nuclear waste stockpiles. The described reactor design makes significant strides on both fronts, by maximizing burnup to reduce the waste production rate, and in doing so limiting the requirement of future repositories.

As shown in Figure 9, fuel burnup and waste production exhibit an inverse power relationship, meaning that the effect of increased burnup on waste production depends highly on the reference position. With a 100% fuel utilization being equivalent to 909 GWd/MTHM and current LWR achieving burnups on the order of 45 GWd/MTHM, it is clear that there remains substantial room for improvement.

To fully explore the goal of maximizing burnup in the MSR, in addition to the fuel cycle cases discussed above, an identical depletion calculation was run for a fuel cycle in line with the enrichment levels proposed by other advanced reactor developers: a 10% enriched initial fuel load with a 20% enriched feed. Figure 10 compares the results of this calculation and those discussed previously in terms of the MSR's improvement over current LWR technology.

As shown in Figure 10, higher enrichments lead to higher burnups, and therefore less waste, due to their ability to maintain criticality for longer periods of time. At the highest LEU enrichment levels, this ability results in an 83% reduction in annual waste production over LWRs. Even under the current industry fuel cycle regime of a 5% enriched initial load with a 5% feed, the MSR reduces annual waste production by approximately 53%.

Further details on the calculations used to determine the MSR's fuel cycle profile can be found in Appendix D.

### *Conclusion*

The MSR design takes advantage of its liquid fuel to allow for more than twice the fuel utilization of light water reactors, leading to an approximately 53% reduction in waste when using 5% enriched uranium, the maximum enrichment readily available in the current supply chain. Using higher enrichments, up to the 20% LEU limit, this reduction reaches 83%. These accomplishments represent major leaps

forward, inverting commonly-held beliefs about the nature of nuclear technology, and enabling nuclear energy to be a viable source of carbon-free baseload power.

### *Appendix A: Calculation Details*

All data presented in this report were generated using the Monte Carlo neutronics software Serpent 2.26.

### *Geometry*

The geometry modeled throughout the report is a 3-dimensional, 3 cm pitch, 7 by 7 rod assembly, as seen depicted in Figure 11. The $ZrH_{1.66}$ moderator rod radius is 1.25 cm, and the rod insertion order used in the simulations is illustrated by the number located in the center of each rod, with 1 indicating the first rod inserted and 49 the last. It should be noted that 4 and 5 cm-pitch models produce similar results, and may be chosen moving forward to limit the total number of rods in the reactor.

### *Materials*

A summary of the material compositions used throughout the simulations is given in Table A.1. Calculations using graphite cladding were also performed and show similar results. For simplicity, only one fuel example (5% LEU) is presented in Table A.1.

**Table A.1.** A summary of material compositions and densities used in the simulations referenced throughout the report. The weight fractions listed are relative to the individual materials and are not representative of the system as a whole.

| Fuel Salt (5.01 g/cm$^3$) | | Silicon Carbide (3.21 g/cm$^3$) | | Zirconium Hydride (5.66 g/cm$^3$) | |
|---|---|---|---|---|---|
| *Isotope* | *Weight Fraction* | *Isotope* | *Weight Fraction* | *Isotope* | *Weight Fraction* |
| $^{235}$U | 3.1100E-02 | $^{12}$C | 2.9936E-01 | $^{90}$Zr | 4.9793E-01 |
| $^{238}$U | 5.9090E-01 | $^{28}$Si | 6.4365E-01 | $^{91}$Zr | 1.0980E-01 |
| $^{7}$Li | 4.8358E-02 | $^{29}$Si | 3.3866E-02 | $^{92}$Zr | 1.6967E-01 |
| $^{6}$Li | 2.4180E-06 | $^{30}$Si | 2.3120E-02 | $^{94}$Zr | 1.7369E-01 |
| $^{19}$F | 3.2964E-01 | | | $^{96}$Zr | 2.8908E-02 |
| | | | | $^{1}$H | 1.8007E-02 |
| | | | | $^{2}$H | 4.1389E-06 |

### *Boundary Conditions*

In order for the model to better represent the core configuration, the simulations invoked reflective boundary conditions, allowing for simulation of an

infinite array of the defined assembly (Figure 11). Leakage considerations as a result of this infinite lattice are discussed further in Appendix B.

### *Cross-Section Libraries*

All cross sections used in the calculations were obtained through the evaluated nuclear data file data base ENDF-VII.1. Scattering kernels for zirconium hydride are not provided by default in Serpent 2.26, and therefore additional data from MCNP was converted to the appropriate format.

### *Neutron Population*

All assembly level calculations discussed were modeled using a simulated population of 10,000 neutrons per cycle, for 30 inactive and 300 active cycles. The statistical error associated with this level of convergence is on the order of $\pm 0.0006$ and 0.0004 for the analog and implicit $k_\infty$ values of each time step respectively.

## Fission Product Removal

The fission product removal rates used in the simulations can be seen below in Table A.2.

**Table A.2.** The fission product removal rates implemented in the depletion calculations discussed previously.

| Element | Removal Rate (atoms/second) | Element | Removal Rate (atoms/second) | Element | Removal Rate (atoms/second) |
|---|---|---|---|---|---|
| H | 5.00E-2 | Br | 1.93E-7 | Sn | 5.79E-8 |
| Ca | 3.37E-9 | Kr | 5.00E-2 | Sb | 5.00E-2 |
| Sc | 3.37E-9 | Rb | 3.37E-9 | Te | 5.00E-2 |
| Ti | 3.37E-9 | Sr | 3.37E-9 | I | 1.93E-7 |
| V | 3.37E-9 | Y | 2.31E-7 | Xe | 5.00E-2 |
| Cr | 3.37E-9 | Zr | 5.79E-8 | Cs | 3.37E-9 |
| Mn | 3.37E-9 | Nb | 5.00E-2 | Ba | 3.37E-9 |
| Fe | 3.37E-9 | Mo | 5.00E-2 | La | 2.31E-7 |
| Co | 3.37E-9 | Tc | 5.00E-2 | Ce | 2.31E-7 |
| Ni | 3.37E-9 | Ru | 5.00E-2 | Pr | 2.31E-7 |
| Cu | 3.37E-9 | Rh | 5.00E-2 | Nd | 2.31E-7 |
| Zn | 3.37E-9 | Pd | 5.00E-2 | Pm | 2.31E-7 |
| Ga | 3.37E-9 | Ag | 5.00E-2 | Sm | 2.31E-7 |
| Ge | 3.37E-9 | Cd | 5.79E-8 | Eu | 2.31E-7 |
| As | 3.37E-9 | In | 5.79E-8 | Gd | 2.31E-7 |
| Se | 5.00E-2 | | | | |

### *Time Step*

In depletion calculations for systems out of equilibrium, it is important to ensure that the initial time steps are short enough to properly simulate the initial evolution of the different actinide vectors. As a result, exponential progression in the size of the steps, as shown in Equation A.1, is common practice, with the current simulations beginning with an initial step of 0.1 days ($\Delta t_1$), increasing by a factor of 1.5 for each subsequent step ($n$).

$$\Delta t = \Delta t_1 \cdot 1.5^{n-1} \quad \text{(A.1)}$$

Over the course of operation, fuel addition and SVF continually disrupt this aforementioned equilibrium, and it is therefore also important to limit the size of the maximum allowable time step. For all results discussed previously, 6 months was chosen as the maximum step limit ($\Delta t_{max}$), with an even more accurate estimation into the final burnup values coming through the use of a Richardson extrapolation (A.2).

$$B_N = \frac{4B_N(\Delta t_{max}) - B_N(2\Delta t_{max})}{3} \quad \text{(A.2)}$$

By running a second depletion calculation with a maximum time step of 12 month ($2\Delta t_{max}$) and extrapolating in combination with the previous 6 month results, the uncertainty associated with the final burnup values is drastically reduced.

### *Appendix B: Leakage Considerations*

In order to limit excess reactivity and achieve a high conversion ratio at the beginning of life, the initial SVF must be very high, on the order of 0.9 for a 5% initial load. As a result, the neutron spectrum at the beginning of life is hardened compared to that of the end of life, as shown in Figure 12.

To accurately model such a spectrum, unresolved resonance probability tables were included in the calculations for several significant isotopes: $^{235}$U, $^{238}$U, $^{238}$Pu, $^{239}$Pu $^{240}$Pu, $^{241}$Pu, and $^{242}$Pu. The omission of other actinides in this consideration is not expected to introduce significant error, as their low concentrations over the course of operation minimize their overall influence.

As the leakage rate of the hardened spectrum is expected to be higher than that of the more thermal spectrum at the end of life, $k_\infty$ limits over the course of a depletion calculation must reflect this evolution. Figure 13 shows the estimated $k_\infty$

trend as a function of the number of rods inserted in an assembly, with leakage considerations, both radially and axially, being obtained by comparing the $k_\infty$ of the infinite assembly to that of a representative three-dimensional core, as shown in Figure 14.

Acting as a complement to Figure 13, Figures 15 and 16 show the radial flux profile of the reactor at the BOL for a 5% enriched initial actinide load, and the Shannon entropy as a function of the number of inactive cycles, respectively.

### *Appendix C: Isotopic Evolution*

In stationary rod configurations, conversion ratio is expected to increase over time as a result of the evolving plutonium vector: plutonium's fissile isotopes (e.g. $^{239}$Pu and $^{241}$Pu) produce both more neutrons, and greater energy per fission than that of $^{235}$U, as well as $^{240}$Pu possesses a significantly higher capture cross section at lower energies (< $10^{-5}$ MeV) than that of $^{238}$U. In a moveable rod method, this effect is outweighed by increased moderation, producing a thermalized spectrum at the end of life (see Figure B.1), which is unfavorable for conversion.

Figure 17 shows the evolution of some of the primary fissile and fertile isotopes as a results of this changing neutron spectrum.

The effect of the moveable rods is most visible upon examination of the sharp decrease in $^{239}$Pu. After roughly 30 GWd/MTHM, $^{239}$Pu surpasses $^{235}$U as the primary contributor to fission in the core, as shown in Table C.1. In addition to this larger consumption rate, $^{238}$U capture can also be seen to drastically decrease over the course of life, as shown in Table C.2, reducing the production rate of $^{239}$Pu.

**Table C.1.** Relative fission rate fraction for the three primary fissile isotopes as a function of burnup. The remaining fraction is a combination of $^{238}$U fast fission and higher-actinides.

| | Burnup (GWd/MTHM) | | | | | | |
|---|---|---|---|---|---|---|---|
| Isotope | *0* | *15* | *30* | *45* | *60* | *75* | *90* |
| $^{235}$U | 0.93 | 0.56 | 0.42 | 0.31 | 0.24 | 0.20 | 0.18 |
| $^{239}$Pu | 0.06 | 0.33 | 0.43 | 0.50 | 0.52 | 0.52 | 0.50 |
| $^{241}$Pu | 0.00 | 0.03 | 0.06 | 0.11 | 0.15 | 0.19 | 0.25 |

**Table C.2.** Relative capture rate as a function of burnup for $^{238}$U. The data are normalized to the $^{238}$U capture rate at the beginning of life.

| | Burnup (GWd/MTHM) | | | | | | |
|---|---|---|---|---|---|---|---|
| Isotope | *0* | *15* | *30* | *45* | *60* | *75* | *90* |
| $^{238}$U | 1 | 0.89 | 0.81 | 0.76 | 0.71 | 0.63 | 0.50 |

## Appendix D: Waste as a Function of Burnup

The relationship between high level actinide waste production and burnup can be derived using the definitions given in Table D.1 and Equations D.1 – D.3. Table D.2 shows that four potential fuel cycles were evaluated in this analysis. Each fuel cycle contains different underlying assumptions about actinide mass and net waste – these assumptions are listed in Tables D.3 and D.4, respectively. Table D.5 gives the resulting net waste production rates for the four fuel cycles.

**Table D.1.** Variable Legend

| | | | |
|---|---|---|---|
| $Bu$ | Burnup | $M_I$ | Initial actinide mass |
| $CL$ | Cycle length | $M_T$ | Total actinide cycle mass |
| $\bar{E}_F$ | Average energy release per fission | $N_A$ | Avogadro's number |
| $\bar{M}$ | Average molar mass per fission | $P$ | Thermal power |
| $M_A$ | Added actinide mass | $\dot{W}_C$ | Waste consumption rate |
| $M_C$ | Consumed actinide mass | $\dot{W}_P$ | Waste production rate |
| $M_E$ | End of cycle actinide mass | $\dot{W}_{P,net}$ | Net waste production rate |

$$\dot{W}_P = \frac{M_E}{CL} \tag{D.1}$$

$$Bu = \frac{P \cdot CL}{M_T} \tag{D.2}$$

$$M_C = \frac{P \cdot CL \cdot \bar{M}}{\bar{E}_F \cdot N_A} \tag{D.3}$$

**Table D.2.** Fuel Cycles

| Case Number | Initial Load | Feed Material |
|---|---|---|
| 1 | LEU | --- |
| 2 | LEU | LEU |
| 3 | LEU | SNF |
| 4 | SNF | SNF |

**Table D.3.** Actinide mass assumptions used in deriving the waste production rate equations given in Table D.5.

| Case Number | Mass Assumptions |
|---|---|
| 1 | $M_E = M_I - M_C \;\&\; M_T = M_I$ |
| 2, 3 & 4 | $M_A \approx M_C, M_I \approx M_E \;\&\; M_T = M_I + M_A$ |

**Table D.4.** Net waste assumptions used in deriving the waste production rate equations given in Table D.5.

| Case Number | Net Waste Assumptions |
|---|---|
| 1, 2 | $\dot{W}_{P,Net} = \dot{W}_P$ |
| 3 | $\dot{W}_{P,Net} = \dot{W}_P - \dot{W}_C \;\&\; \dot{W}_C = \frac{M_A}{CL}$ |
| 4 | $\dot{W}_{P,Net} = -\dot{W}_C \;\&\; \dot{W}_C = \frac{M_A}{CL}$ |

**Table D.5.** Waste production rate equations for the fuel cycles presented in Table D.2.

| Case Number | Final Formulation |
|---|---|
| 1 & 2 | $\dot{W}_{P,Net} = \frac{P}{Bu} - \frac{P \cdot \bar{M}}{\bar{E}_F \cdot N_A}$ |
| 3 | $\dot{W}_{P,Net} = \frac{P}{Bu} - 2\frac{P \cdot \bar{M}}{\bar{E}_F \cdot N_A}$ |
| 4 | $\dot{W}_{P,Net} = -\frac{P \cdot \bar{M}}{\bar{E}_F \cdot N_A}$ |

Case 4 has a negative waste production rate, which means that it consumes nuclear waste on net. In cases 1, 2, and 3, burnup appears directly in the equations for net waste production. Burnup does not appear directly in the equation for case 4, but it is still an important parameter for evaluating the fuel cycle. The waste produced by the described MSR has a lower fissile composition than the waste produced by a light water reactor (1.2% fissile versus 2% fissile), and therefore cannot be reused in subsequent core loadings. Maximizing burnup is therefore crucial for minimizing the quantity of new nuclear waste production, and achieving higher burnups will even more rapidly reduce worldwide stockpiles of nuclear waste.

A number of embodiments of the invention have been described. Nevertheless, it will be understood that various modifications may be made without departing from the spirit and scope of the invention. Accordingly, other embodiments are within the scope of the following claims.

**WHAT IS CLAIMED IS:**

1. A molten salt reactor comprising:
a core with a variable geometry.

2. The molten salt reactor of claim 1 comprising moveable moderator elements.

3. The molten salt reactor of claim 2 wherein the moveable moderator elements comprise moveable moderator rods.

4. A method of operating a molten salt reactor comprising controlling reactivity of the reactor by controlling geometry of a core of the reactor.

5. The method of claim 4, comprising removing fission products from the core of the reactor.

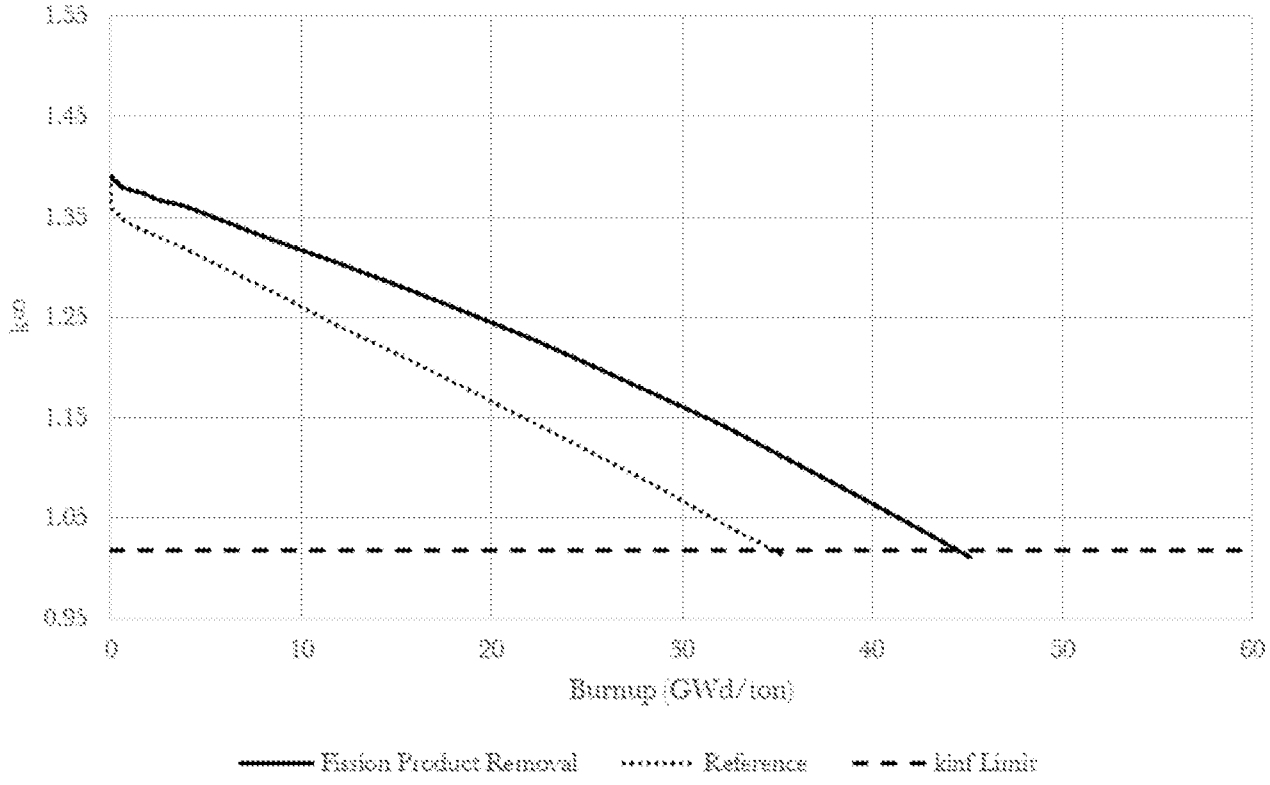


Figure 1

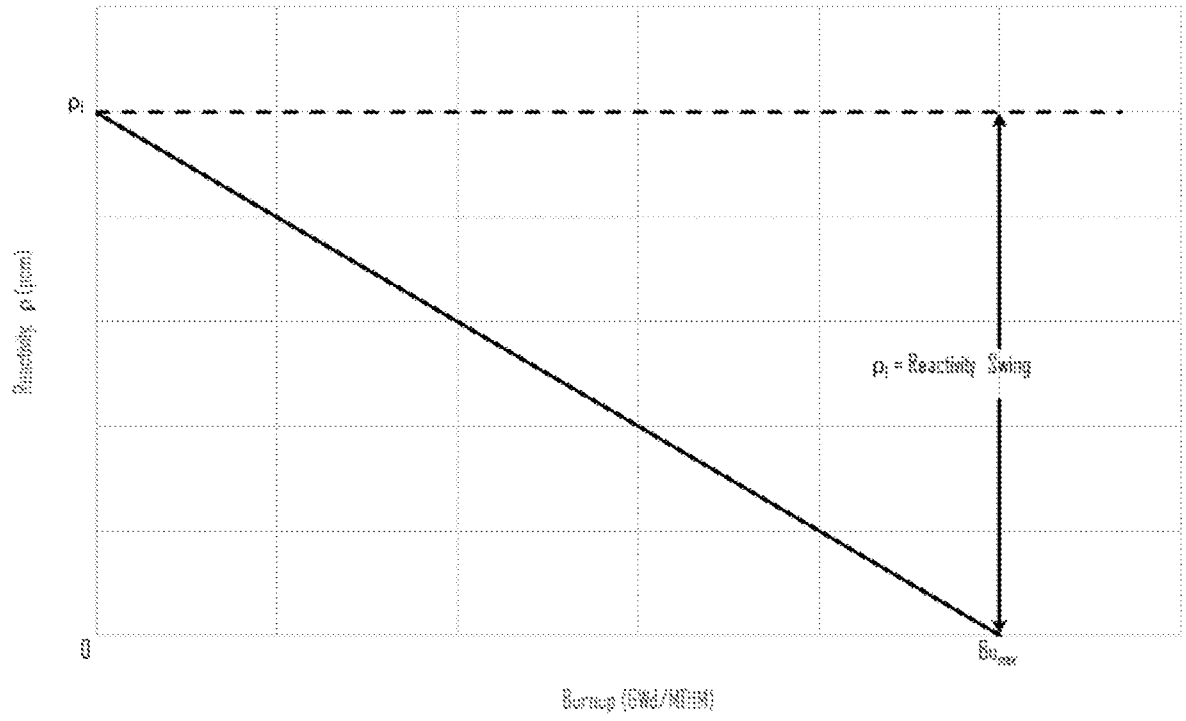


Figure 2

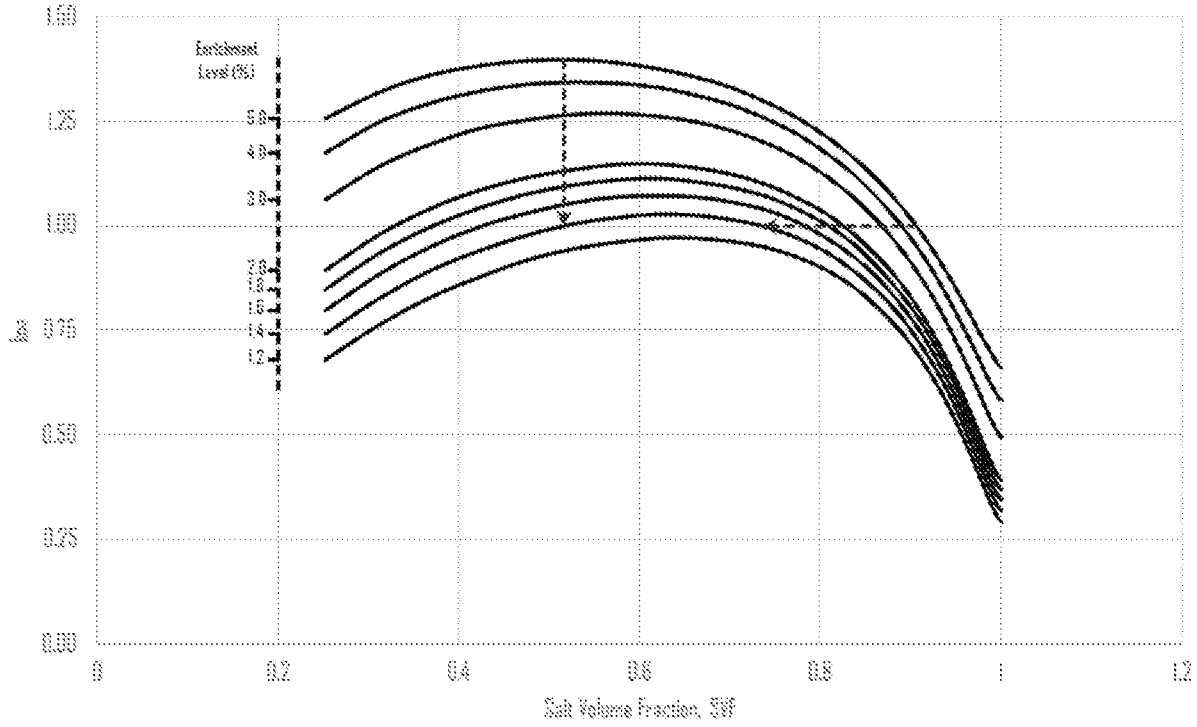


Figure 3

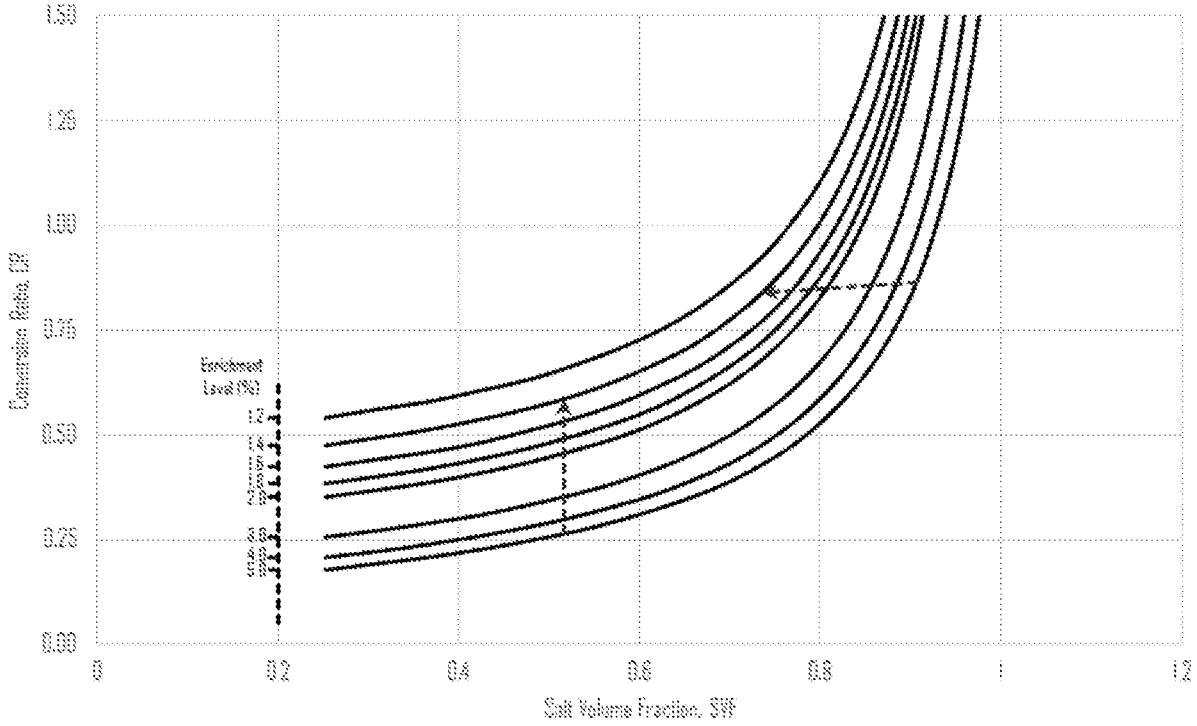


Figure 4

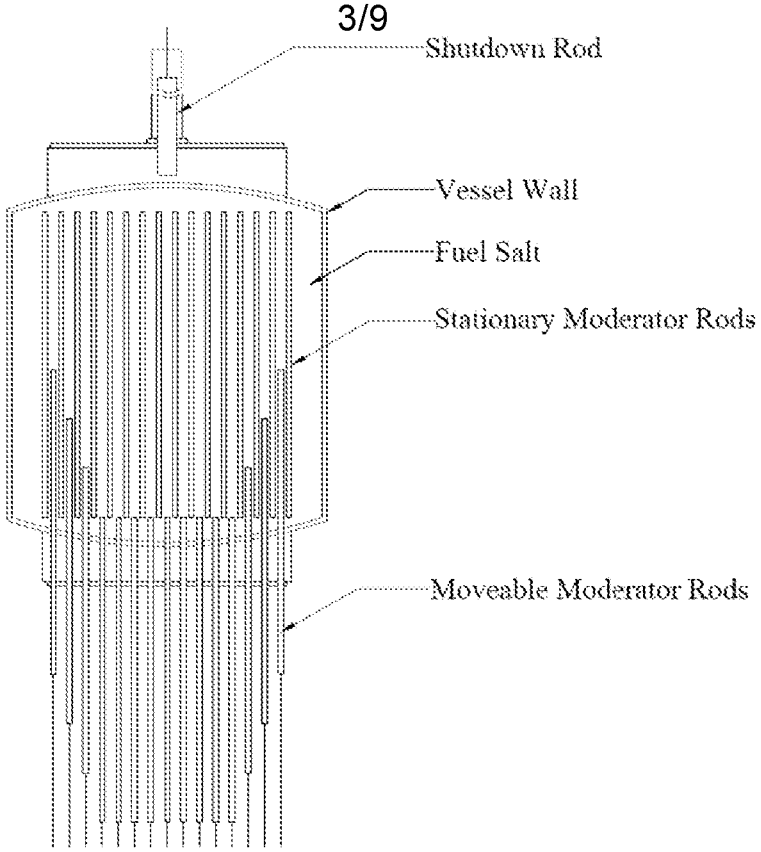


Figure 5

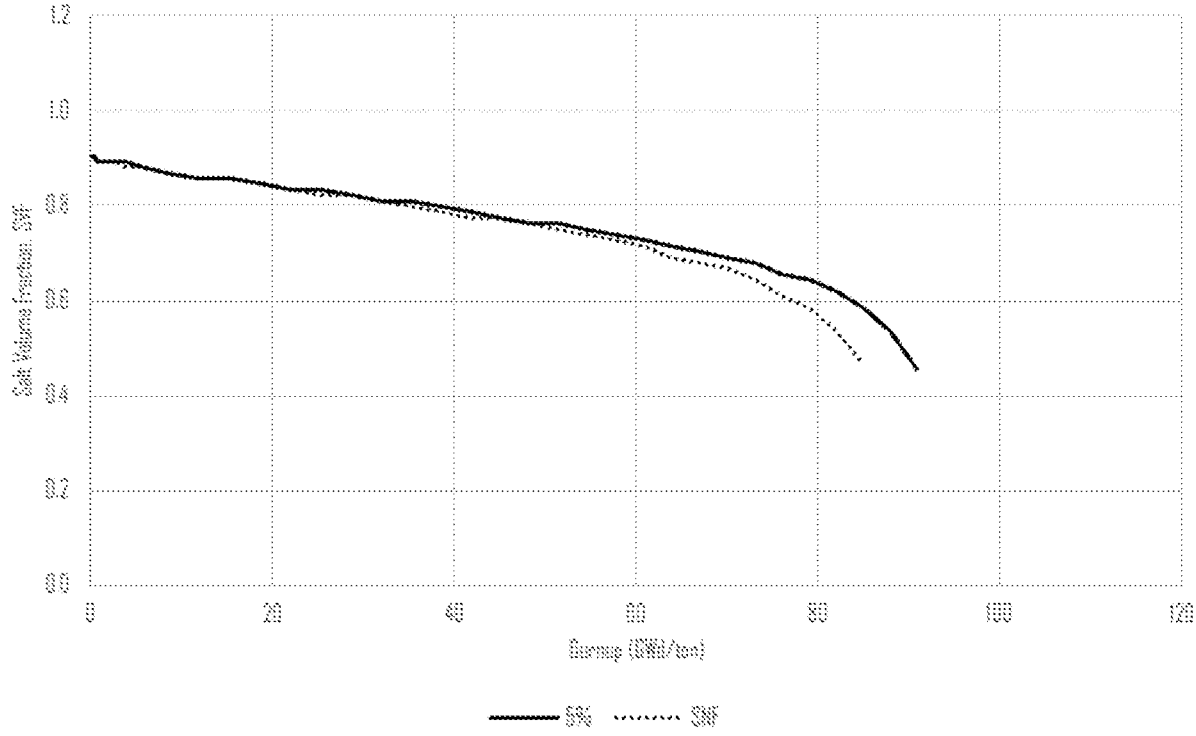


Figure 6

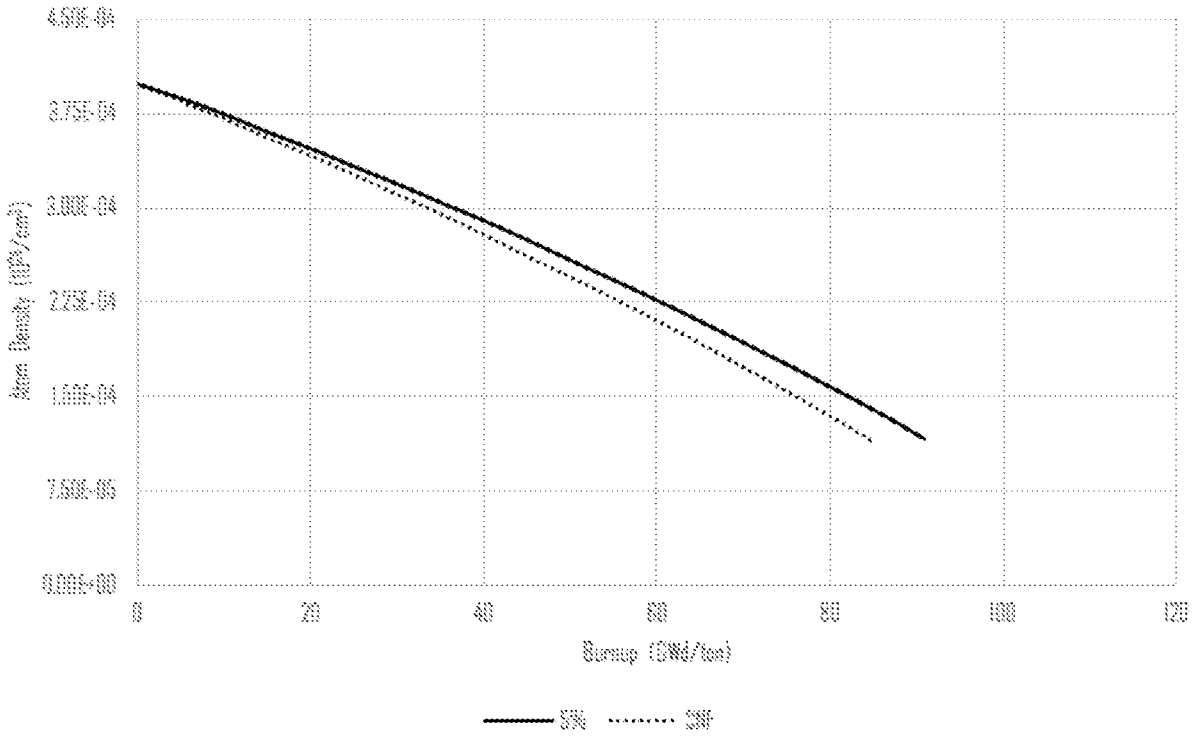


Figure 7

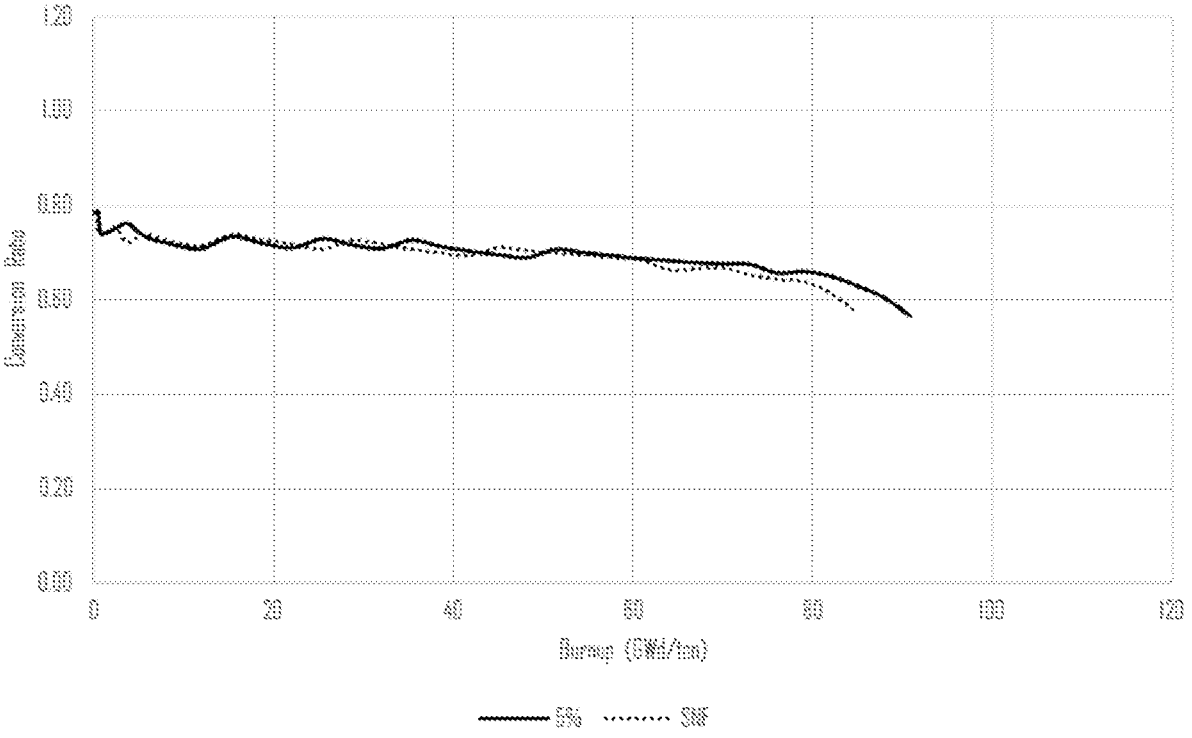


Figure 8

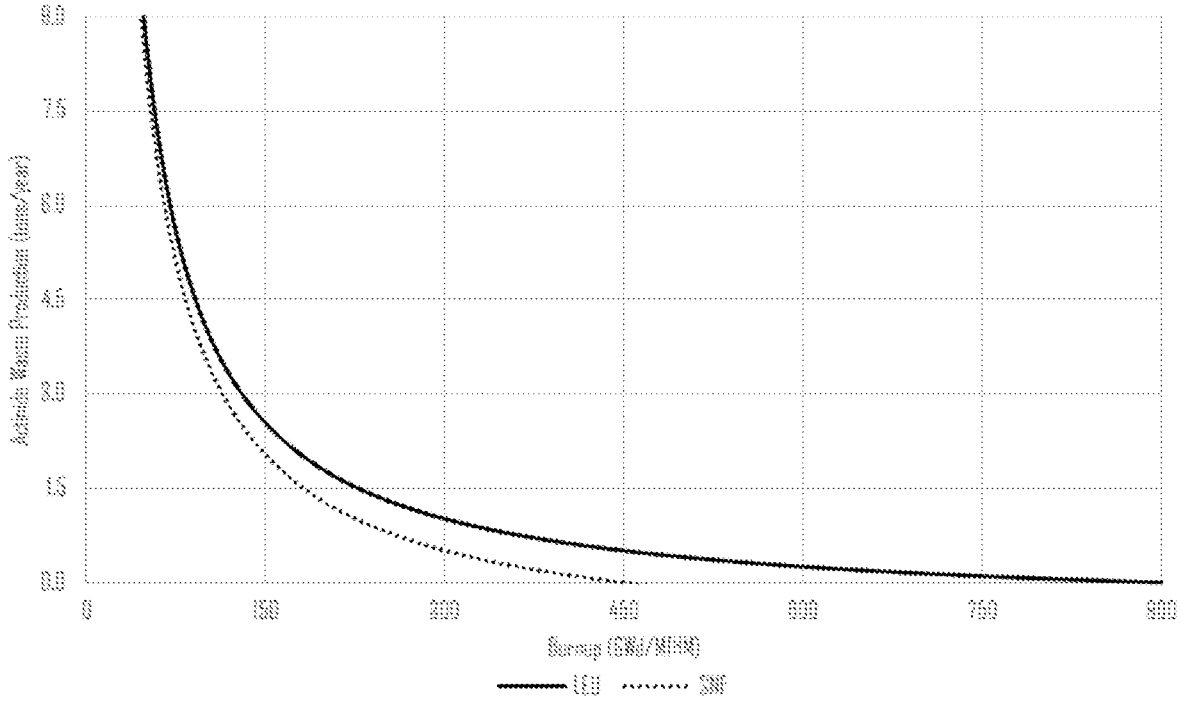


Figure 9

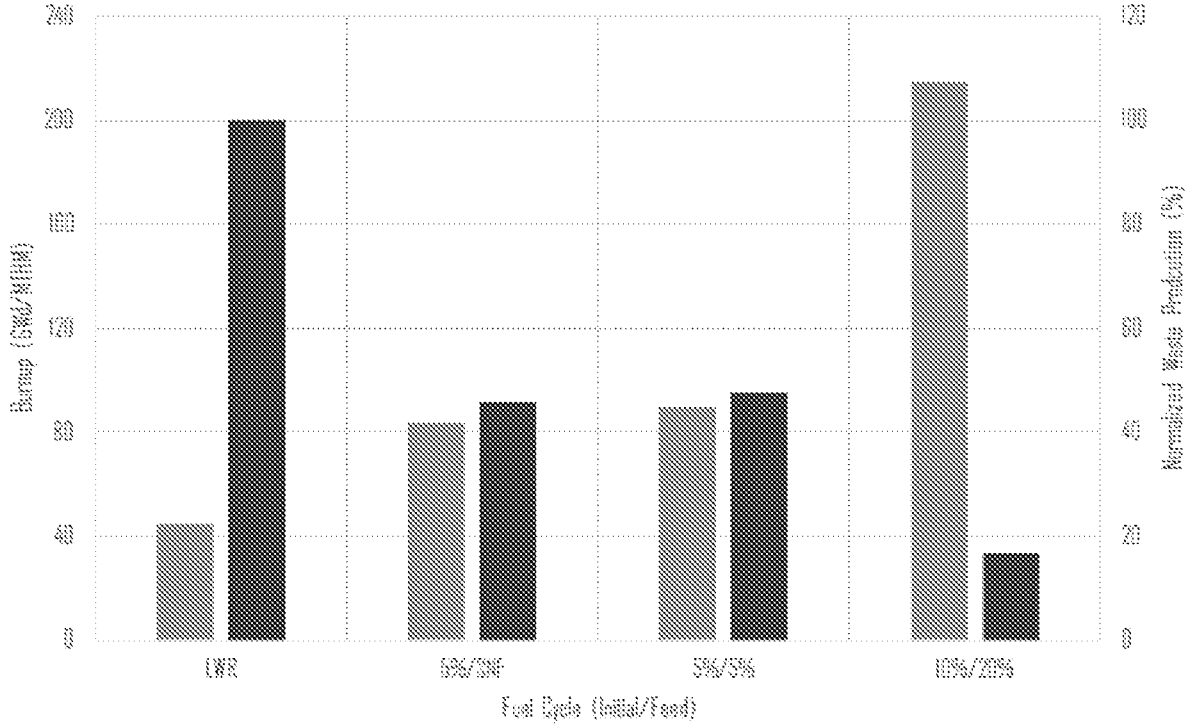


Figure 10

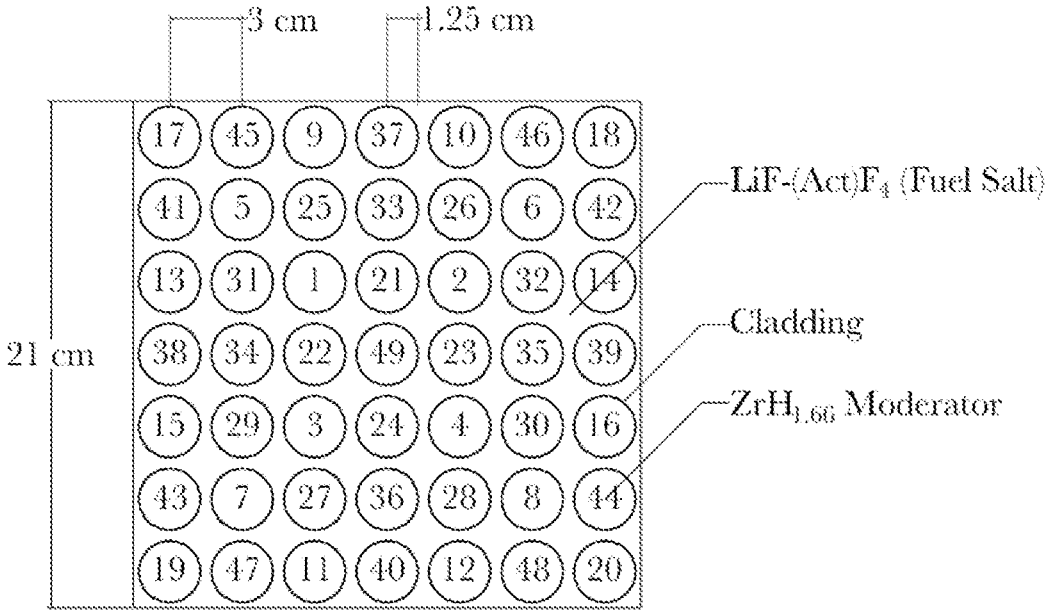


Figure 11

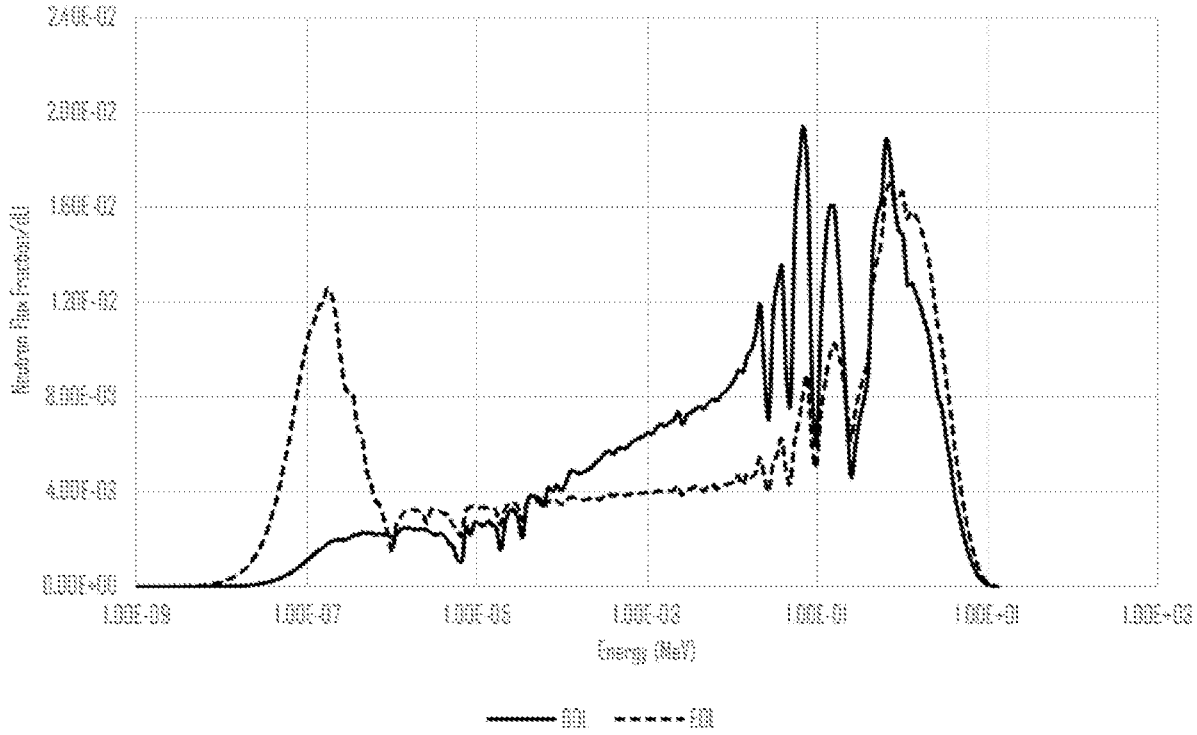


Figure 12

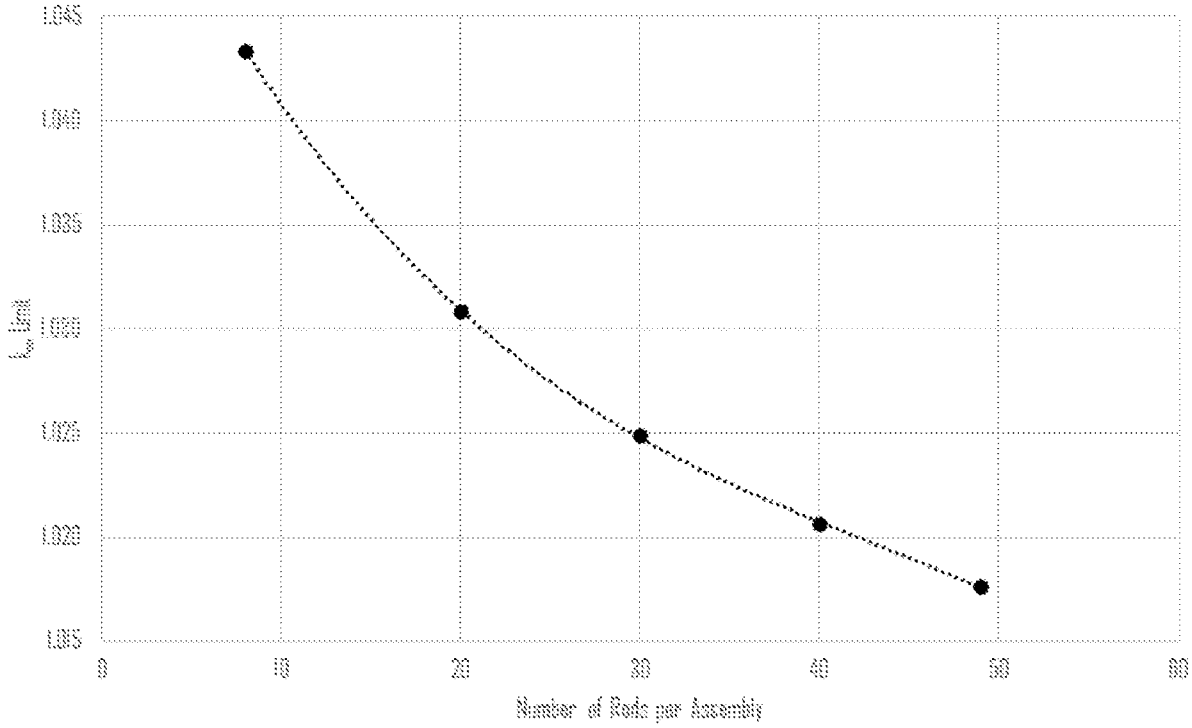


Figure 13

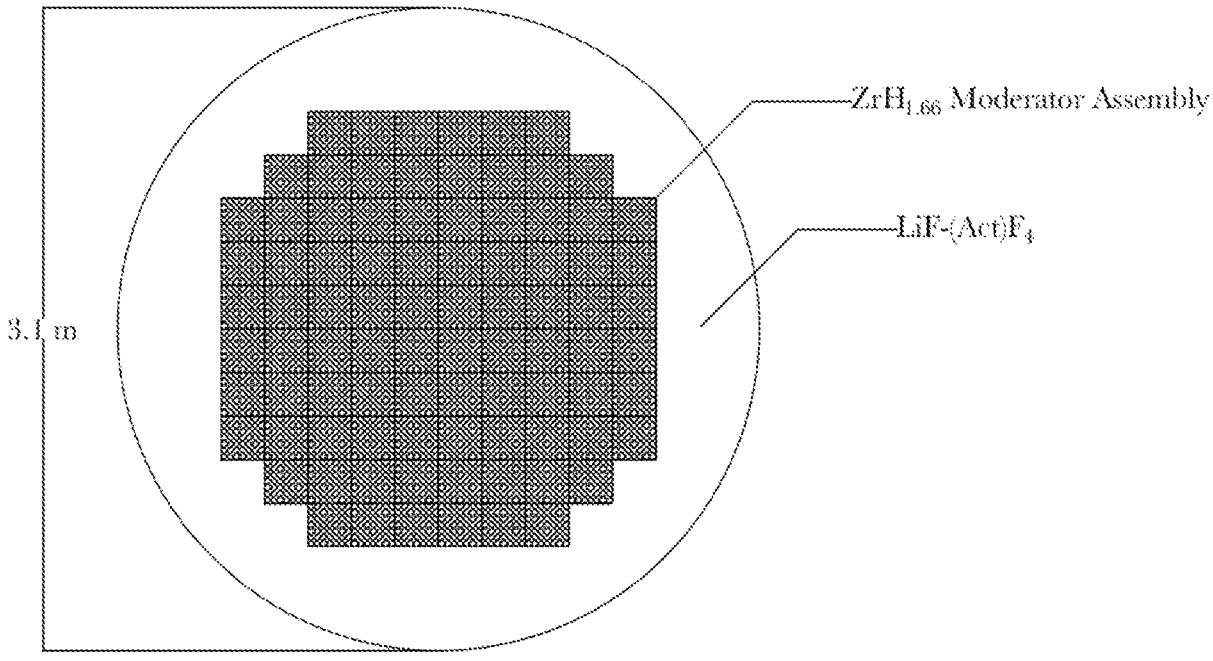


Figure 14

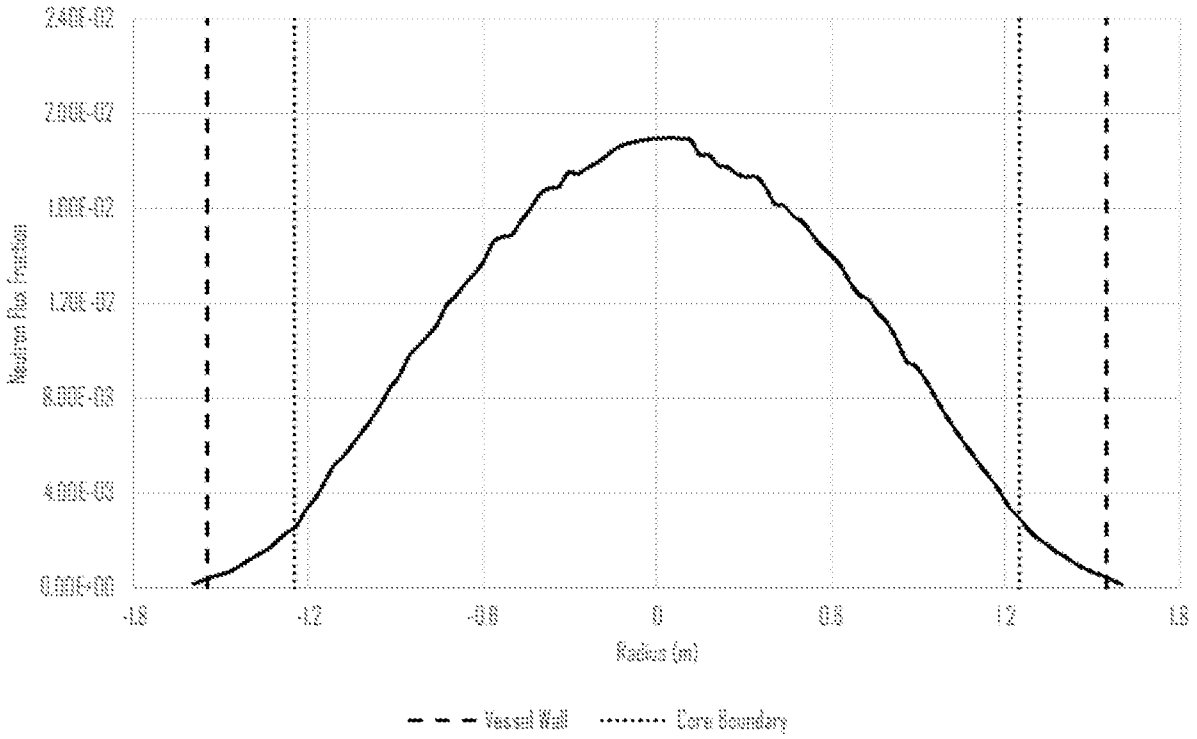


Figure 15

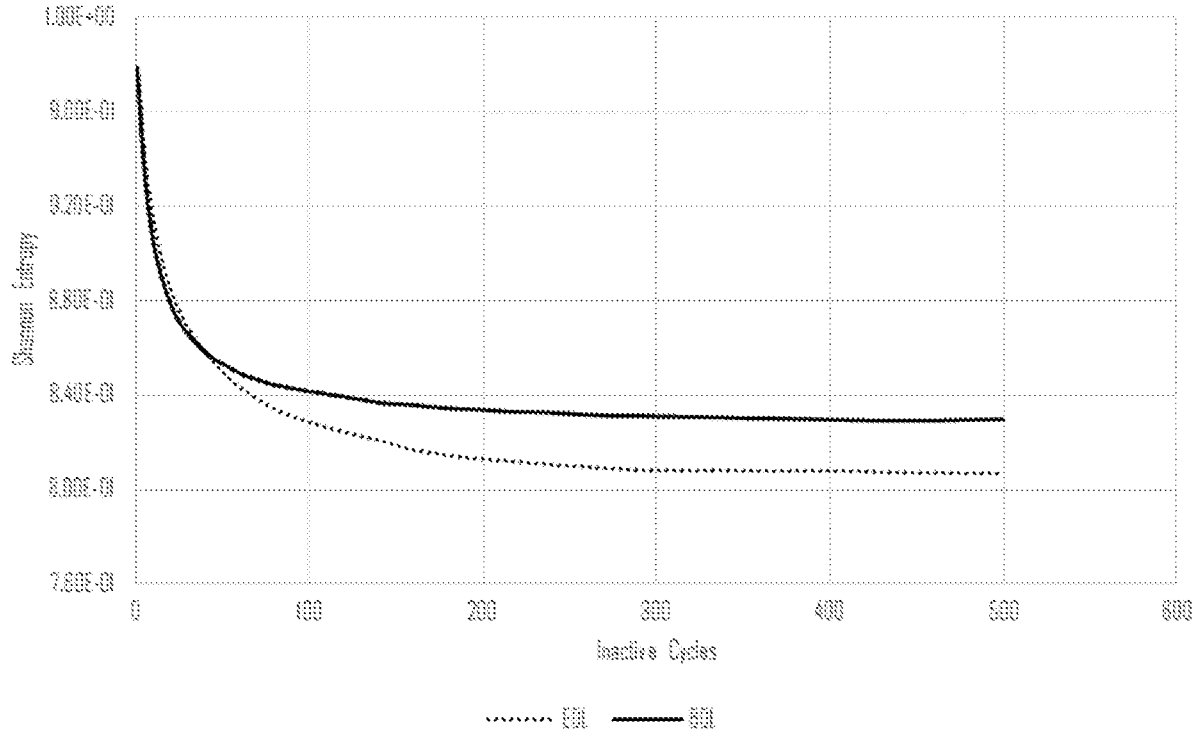


Figure 16

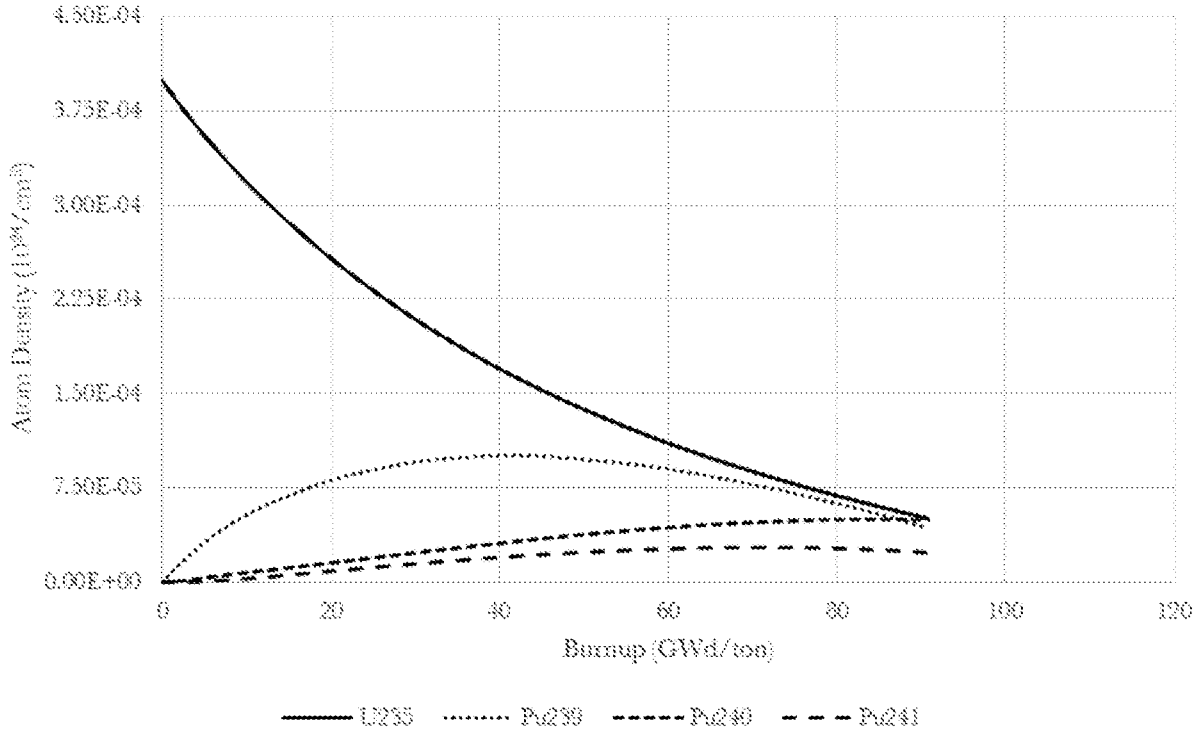
4.50E-04
3.75E-04
3.00E-04
2.25E-04
1.50E-04
7.50E-05
0.00E+00
Atom Density (10^24/cm^3)
0
20
40
60
80
100
120
Burnup (GWd/tee)
U235
Pu239
Pu240
Pu241

Figure 17